Dynamics of nanoparticle assembly from disjointed images of nanoparticle-polymer composites

Chaitanya R. Murthy, Bo Gao, Andrea R. Tao, and Gaurav Arya

Phys. Rev. E **93**, 022501 — Published 18 February 2016

DOI: 10.1103/PhysRevE.93.022501

Dynamics of nanoparticle assembly from disjointed images of nanoparticle-polymer composites

Chaitanya R. Murthy, Bo Gao, Andrea R. Tao, and Gaurav Arya*

Department of NanoEngineering, University of California, San Diego

Abstract

Understanding how nanoparticles (NPs) diffuse, stick, and assemble into larger structures within polymers is key to the design and fabrication of NP-polymer composites. Here we describe an approach for inferring the dynamic parameters of NP assembly from spatially and temporally disjointed images of composites. The approach involves iterative adjustment of the parameters of a kinetic model of assembly until the computed size statistics of NP clusters match those obtained from high-throughput analysis of the experimental images. Application of this approach to the assembly of shaped, metal NPs in polymer films suggests that NP structures grow via a cluster-cluster aggregation mechanism, where NPs and their clusters diffuse with approximately Stokes-Einstein diffusivity and stick to other NPs or clusters with a probability that depends strongly on the size and shape of the NPs and the molecular weight of the polymer.

PACS numbers: 81.16.Dn, 82.35.Np, 83.10.Pp, 87.10.Hk

* garya@ucsd.edu

I. I. INTRODUCTION

The incorporation of nanoparticles (NPs) into polymers is a powerful strategy for enhancing their thermomechanical properties and for introducing new optical, electrical, and magnetic functionalities into the polymers [1, 2]. Many applications require the incorporated NPs to be assembled into clusters, strings, sheets, and percolating networks to take advantage of their collective properties [3–5]. To achieve control over NP assembly, a complete understanding of how NPs and their clusters diffuse, collide, stick, and grow into larger structures is critical. Several models of colloidal assembly have established the growth rate, morphology, and size distribution of particle assemblies, which are expected to be primarily governed by the diffusivity of the particles and their clusters and the probability with which they stick to each other upon collision [6, 7]. In nanocomposites, these two parameters strongly depend on various chemical and physical properties of the NPs, such as their size, shape, and surface functionalization. Obtaining experimental information regarding these dynamic parameters of NP assembly is highly challenging because it requires real-time imaging and quantitative measurements of the nanocomposite during assembly. Such observation requires *in-situ* scanning or transmission electron microscopy [8] to capture rapid events like NP collisions, which has been achieved to some extent for NPs in liquid cells [9–11], but is difficult to achieve for polymer-embedded NPs.

In this paper, we show that it is possible to extract useful kinetic information about the NP assembly process from temporally and spatially disjointed images of NP composites, typically obtained from distinct samples arrested at different stages of assembly. Our approach involves adjustment of the parameters of an appropriate kinetic model of NP assembly until the computed size distributions of the NP clusters reproduce those obtained from quantitative analysis of the experimental images. We apply this approach to determine the dynamic parameters—diffusivity scalings and sticking probabilities—governing the assembly of metal NPs of varying shapes and sizes within polymer films of varying molecular weight. Our results reveal certain universality in the mechanism by which NPs diffuse and assemble in a polymer film as well as interesting dependencies on the shapes and sizes of the NPs and the chain length of the surrounding polymer.

II. II. ASSEMBLY EXPERIMENTS

To demonstrate our approach, we applied it to five different sets of experiments involving polymer-grafted metal NPs undergoing two-dimensional assembly within a polymer thin film. The experiments differ in the size and shape of the NP undergoing assembly and in the molecular weight of the surrounding polymer matrix. Table I provides relevant properties of the NPs, NP-grafts, and matrix polymer used in the experiments.

TABLE I. Relevant parameters for the five experimental systems investigated in this study.

NP type	Size[a]	Graft, Mw[b]	Matrix, Mw
Silver (Ag) cubes	80 (e)	PVP[c], $55k$	PS[d], $11k$
Gold (Au) rods	$40, 10$ (l, d)	PVP, $55k$	PS, $11k$
Gold spheres	10 (d)	PVP, $55k$	PS, $11k$
Silver spheres	30 (d)	PVP, $55k$	PS, $3k$
Silver spheres	30 (d)	PVP, $55k$	PS, $28k$

[a] e: edge length, d: diameter, l: axial length, each in nm

[b] Mw: molecular weight in Daltons (k stands for kilo)

[c] PVP: poly(vinyl pyrrolidone), [d] PS: polystyrene

Details of NP synthesis, assembly, and imaging are provided elsewhere [12]; here we provide only the most essential information. In brief, we used standard wet chemical methods to synthesize shaped NPs of uniform size and surface-functionalized with poly(vinyl pyrrolidone) chains. The colloidal dispersion of NPs was spread onto an air-water interface to produce a monolayer of uniformly distributed NPs, which was then transferred onto the surface of a thin polystyrene film. Solvent annealing was used for embedding the NPs into the underlying polymer. This caused the NPs to sink into the film and begin to diffuse within it and assemble into larger NP clusters. For each experimental system, we captured around 100 scanning electron microscopy (SEM) images spread over multiple time points across the assembly. Figure 1 presents representative SEM images captured at different time points during experiments involving the assembly of silver nanocubes.

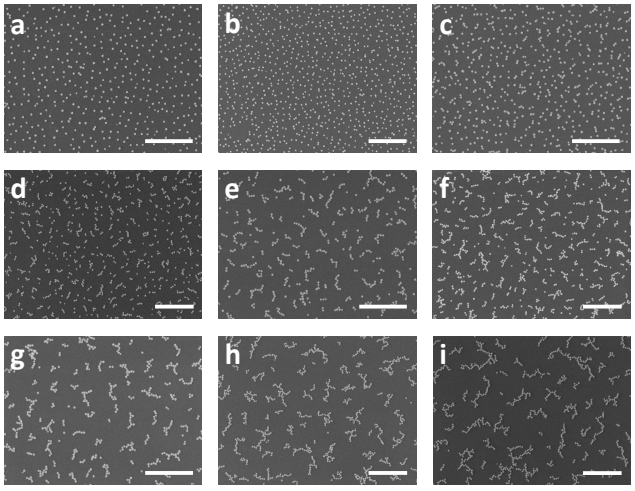

FIG. 1. Representative SEM images taken during the assembly of 80 nm PVP-grafted Ag nanocubes within PS thin film at the following times post solvent annealing: (a) 127 min, (b) 135 min, (c) 143 min, (d) 150 min, (e) 158 min, (f) 165 min, (g) 173 min, (h) 180 min, and (i) 188 min. Scale bar = 2 μm.

III. III. KINETIC MODEL

To choose an appropriate kinetic model of NP assembly, we turned to the various models developed over the years to describe colloidal aggregation. The cluster-cluster aggregation (CCA) model [13, 14] is one of the simplest but most versatile of these models; it has been shown to yield qualitatively correct descriptions of the aggregation dynamics and aggregate morphologies observed in a wide range of colloidal systems. In its simplest form, CCA consists of a collection of diffusing particles that stick together irreversibly upon contact to form clusters; these clusters continue to diffuse and grow by colliding with other particles or clusters. The model can also be easily extended to include additional features like size-dependent cluster mobilities and variable sticking probabilities, which have been thoroughly studied [6, 15].

Based on this model, a dynamic scaling form for the cluster size distribution function was introduced [16]:

$$n_s(t) \sim s^{-2} \mathcal{F}\left(s/t^z\right), \tag{1}$$

where $n_s(t)$ is the number density of clusters containing s particles at time t, $\mathcal{F}$ is a scaling

function, and z is a critical exponent. It was also shown that the mass-average cluster size

$$S(t) = \frac{\sum s^2 n_s(t)}{\sum s n_s(t)} \tag{2}$$

scales as $S(t) \sim t^z$ as $t \to \infty$. Subsequent experiments demonstrated and studied this dynamic scaling of the size distribution in various colloidal systems [17–19]. Both the CCA model and the arguments leading to the dynamic scaling form are simple and general, and should therefore be widely applicable. However, to our knowledge, Eq. (1) has not previously been tested for the case of NPs assembling in a polymer matrix, despite the widespread study of such NP-polymer systems.

To investigate the applicability of this scaling relationship to NP assembly, we analyzed the different sets of experiments described earlier involving the assembly of polymer-grafted metal NPs within a polymer thin film. The size distributions of the NP clusters were obtained by analyzing SEM images of the five polymer-NP systems captured at various stages of assembly. For this purpose, we used an automated image analysis tool that we recently developed and made publicly available [12, 20]. Though studies frequently employ $n_s(t)$ to quantify cluster size distribution, a more useful measure is the *relative* cluster size distribution $\nu_s(t)$ defined as

$$\nu_s(t) = \frac{N_s(t)}{\sum s N_s(t)}, \tag{3}$$

where $N_s(t)$ is the number of clusters containing s particles at time t. The quantity $\nu_s(t)$ normalizes $N_s(t)$ by the total number of particles $\sum s N_s(t)$ across all clusters and therefore allows comparison of the cluster size distributions at different time points, from different experiments, and against those obtained from simulations. Also note that $\nu_s(t)$ is proportional to $n_s(t)$ via $\nu_s(t) = n_s(t)/\Phi$, where Φ is the overall number density of particles in the system, assumed to be constant.

Figure 2 plots the reduced cluster size distributions $s^2\nu_s(t)$ versus reduced cluster size $s/S(t)$ obtained from the five experiments. Most of the data points are found to collapse onto a single master curve, with slight deviations at low cluster sizes and/or long times for the data corresponding to 13 nm spheres and to 30 nm spheres in 3k polystyrene film. Some deviations from absolute universality are expected due to the approximate nature of the dynamic scaling and its obvious failing at very short times, where only single NPs exist, and at very long times, where only a single, large cluster exists [16]. Other plausible reasons include statistical uncertainties in the extracted $\nu_s(t)$ due to the limited number of SEM

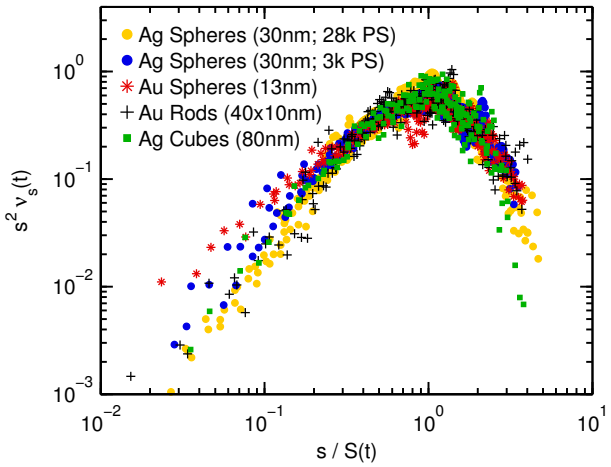

FIG. 2. Evidence of dynamic scaling in NP assembly in two dimensions in a polymer matrix. Reduced cluster size distributions obtained via image analysis of SEM images from five experiments are plotted versus reduced cluster size. Each set of points includes data for all recorded time points in that experiment. The entries in parentheses in the legend indicate the approximate sizes of the NPs and the molecular weight of the polystyrene (PS) matrix (11k PS where not indicated).

images available for analysis and the actual assembly being more complex than the CCA model. Nevertheless, the NP assembly systems studied here still follow reasonably well the cluster size distribution scalings predicted by the CCA model, suggesting some degree of universality in the mechanism by which NPs assemble.

Based on these results, we contend that the CCA model should be able to simulate many important aspects of the assembly process of the different NP-polymer systems studied here and that it would be an appropriate model in our approach for recovering the dynamic parameters of NP assembly. The CCA model takes as input the initial number density of particles along with dynamic parameters that describe the diffusion and sticking of the particles and clusters. By quantitatively comparing cluster size distributions obtained in CCA simulations to those obtained in experiments, we should be able to predict these dynamic parameters. This method is representative of a simple and general framework for gaining quantitative information about the microscopic behavior of NPs in a polymer by analyzing static snapshots taken during their aggregation process and comparing the data with a suitable model.

IV. IV. LATTICE CCA SIMULATIONS

We simulate CCA on a two-dimensional square lattice, in accordance with the thin-film geometry of the experimental system, and implement periodic boundary conditions to prevent boundary effects. A simulation begins with $N_0 < L^2$ particles randomly placed at N_0 sites of an $L \times L$ lattice (no two particles ever occupy the same position). The diffusion of particles and their clusters is treated as a random walk on the lattice. The self-diffusivity D_s of a cluster containing s particles is assumed to scale with the cluster size in a power-law manner [15]:

$$D_s(\gamma) = D_0 s^{\gamma}, \tag{4}$$

where D_0 is a constant denoting the self-diffusivity of single particles and γ is a parameter embodying the size-dependence of the diffusivity on cluster size. The case $\gamma = 0$ corresponds to a size-independent diffusivity, whereas for $\gamma < 0$, larger clusters diffuse slower. Scalings with $\gamma > 0$, where larger clusters diffuse faster, were not considered.

Previous studies on colloidal aggregation [7] have shown that particles can collide unproductively when the inter-particle interaction potentials exhibit an energy barrier that prevent particles from sticking within the residence time of their contact. For the NPs analyzed here, such barriers could arise from steric repulsion between particles due to the polymer chains grafted on the particle surfaces [4, 21]. To this end, we implement a sticking probability P_{stick} between clusters that may be smaller than 1. Following previous work [6, 22], we assign a probability P that two particles arriving at neighboring sites on the lattice stick to form a two-particle cluster. The sticking probability between clusters exhibiting more than one contact points—one or more of its particles occupy lattice sites adjacent (modulo L) to those occupied by particles belonging to other clusters—is then given by [23]

$$P_{\text{stick}} = 1 - (1 - P)^c, \tag{5}$$

where we have assumed that two clusters will stick to each other if any one of the c contacts stick independently with the probability P.

The standard approach for simulating the dynamical evolution of such a system uses a fixed time step of $\Delta t = 1$. At each simulation time step t_i, an attempt is made to move each and every cluster by one lattice unit in a randomly chosen direction with probability $D_{s_k}(\gamma)/D_0$, where s_k is the size of the cluster k being moved and $D_{s_k}(\gamma)$ is its diffusivity

given Eq. (4). Alternatively, the attempts may involve moving only a single, randomly picked cluster per time step with the above probability. In this case, the simulation time should be incremented by $\Delta t_i = 1/N(t_i)$, where $N(t_i)$ is the number of clusters present at the beginning of the time step, to yield the same overall dynamics as the earlier approach. Both these approaches become increasingly inefficient with time for systems with $\gamma < 0$ as clusters grow in size and their diffusivities $D_{s_k}(\gamma)$ become increasingly smaller, leading to diminishing move probabilities. However, significant computational savings may be achieved by a simple modification [15]: multiplying the above move probability by a factor of $D_0/D_{\max}$ (≥ 1), where $D_{\max}$ is the largest diffusion coefficient for any cluster present in the system at the start of the time step. Concurrently, the time step needs to be multiplied by the same factor to achieve similar dynamics as those obtained from the standard approach.

The simulation protocol then proceeds as follows: At each simulation time step t_i, a cluster k is selected at random and moved with probability $D_{s_k}(\gamma)/D_{\max}$ by one lattice unit in a randomly chosen direction. If an attempted move results in double-occupancy of a lattice site, the move is rejected and the cluster remains in its old position. If a move results in cluster k being left in contact with other clusters, then cluster k is merged with each contacting cluster l with probability given by Eq. (5), where $c = c_{kl}$ is the number of contact points between clusters k and l. Regardless of what has occurred during the time step, the time is incremented by

$$\Delta t_i = \frac{D_0}{D_{\max}} \frac{1}{N(t_i)}. \tag{6}$$

At the end of this process, we are left with $N(t_{i+1}) \leq N(t_i)$ clusters with average size $S(t_{i+1}) \geq S(t_i)$. This completes one time step of the simulation. The above process is repeated until the average cluster size exceeds the largest cluster size achieved in the experiments.

The results of the simulations are expected to depend on three parameters:

1. The particle number density $\Phi = N_0/L^2$ (the fraction of lattice sites that are occupied). All simulations were performed with $\Phi = 0.07$, the approximate number density of particles observed in the experiments. We assume that the N_0 and L values used (our smallest simulations used $N_0 = 11200$ and $L = 400$) are large enough that the results presented will not change with increasing system size, keeping Φ constant.

2. The diffusion exponent γ, which determines the size-dependence of cluster diffusivity

via Eq. 4. Values of γ between 0 and -1 were considered.

3. The sticking probability P per contact point. Values of P between 1 and 10^{-3} were considered.

Simulation results for each set of parameters were averaged over $N_R \geq 100$ independent simulation runs.

V. V. RESULTS AND DISCUSSION

We aim to quantitatively compare the cluster size distributions obtained from the CCA simulations (performed using different combinations of γ and P values) with those measured from each of the five experiments to determine the underlying dynamic parameters associated with each experiment. The cluster size distribution in our simulations is computed as $\hat{\nu}_s(t_i) = N_s(t_i)/N_0$, where $N_s(t_i)$ is the number of clusters of size s present at time step t_i, and N_0 is the initial number of particles placed on the lattice; note that N_0 is equivalent to $\sum sN_s(t)$ in Eq. (3). In order to compare simulation to experiment, we define

$$Q_\nu = \frac{1}{\mathcal{N}} \sum_{t,s} \frac{|\nu_s(t) - \hat{\nu}_s(t^*)|}{\sqrt{[\sigma_{\nu_s}(t)]^2 + [\sigma_{\hat{\nu}_s}(t^*)]^2}}, \tag{7}$$

which measures the fit quality or degree of overlap between the experimental and simulation cluster size distributions. The numerator of each term is the absolute difference between $\nu_s(t)$, the experiment cluster size distribution at time t, and $\hat{\nu}_s(t^*)$, the corresponding simulation cluster size distribution (at simulation time t^*); the method by which this correspondence is chosen is described below. The quantities $\sigma_{\nu_s}(t)$ and $\sigma_{\hat{\nu}_s}(t^*)$ in the denominator are the standard deviations of $\nu_s(t)$ and of $\hat{\nu}_s(t^*)$, respectively. The former deviation is calculated as described in Ref. [12], while the latter is obtained using the N_R independent simulation runs. The sum runs over all experiment times and cluster sizes for which experiment data was collected, and $\mathcal{N}$ is the total number of terms in the sum.

Ideally, the simulation time would be related to the experiment time by a constant multiplicative factor τ equal to the timescale for diffusion of the NPs being modeled. In this situation, we could simply fix $t/t^* = \tau$ in Eq. 7, and then determine the value of τ as that which minimizes Q_ν for a given experiment/simulation pair. Unfortunately, experimental conditions render this approach infeasible: NPs are initially deposited on a glassy polymer

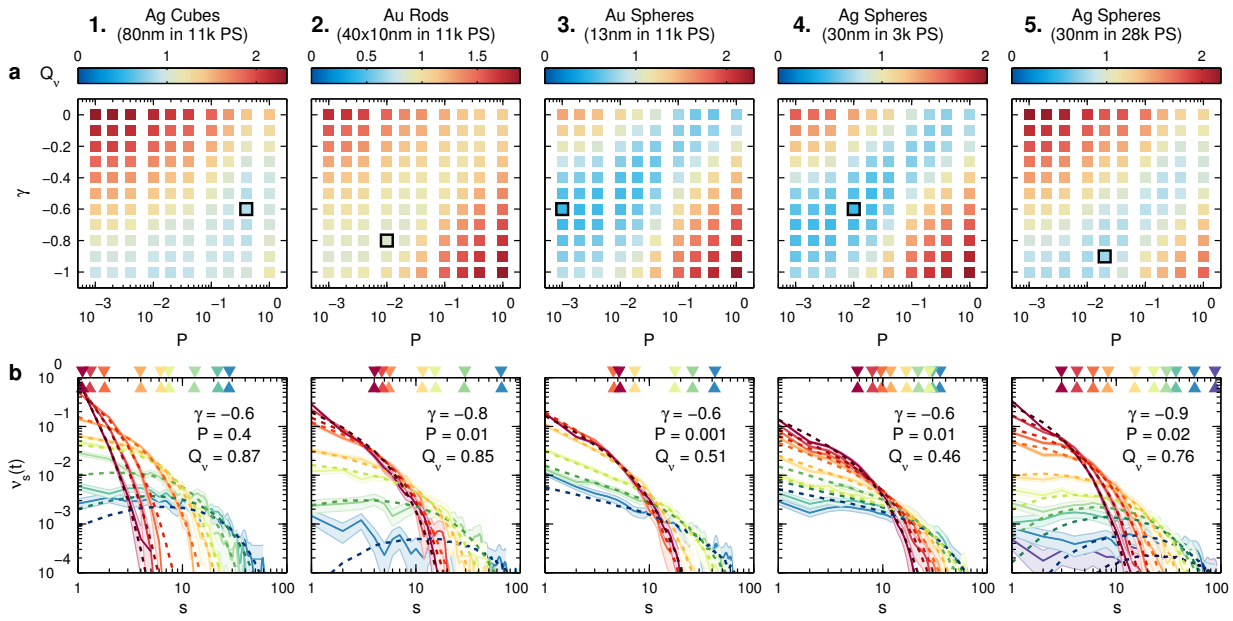

FIG. 3. Results of comparison between experiments and simulations, where each column is for the indicated experiment. (a) Q_ν values for all simulations performed, organized by parameter values (diffusivity scaling γ and sticking probability P). (b) Experimental cluster size distributions (solid lines with error bounds) overlaid with the corresponding simulation size distributions (dashed lines) taken from simulations with the indicated parameters—these are also marked in (a) with black squares. The $\nu_s(t)$ curves are colored from red to blue/purple in order of increasing time. The colored triangles above/below the top of each plot mark the experimental/simulation mass-average cluster sizes, respectively, for each plotted time.

film, and the polymer is then made mobile by exposure to solvent vapor, allowing the NPs to sink in and begin lateral diffusion. This process is not instantaneous, and we observe a long "dormant" period (∼1–2 hours) after solvent exposure begins, before the onset of NP aggregation [12]. It is reasonable to assume that the polymer will continue to swell after this point, and that the NP mobility will therefore continue to rise with time.

To address this problem, we assume that changes in the polymer cause the diffusion constant D_0 to become some arbitrary function of time $D_0(t)$, but that the sticking probability P remains time-independent. According to Eq. 4, this imposition of a time-dependent $D_0(t)$ should affect the diffusion coefficients of all clusters equally, which is equivalent to simply rescaling each simulation time step Δt_i by an appropriate factor. Therefore, the simulation results remain valid, but with each simulation time t_i now mapped in some unknown, non-

trivial way to an experiment time t. In applying Eq. 7, we choose each simulation time t^* so as to minimize the difference between the experimental mass-average cluster size, $S(t)$, and the corresponding simulation value, $\hat{S}(t^*)$.

Figure 3 presents the results of our comparative study. We find that the analysis immediately rules out large sections of the simulation parameter space for each experiment (red and yellow zones in Fig. 3a). The remaining (blue) regions, where Q_ν is relatively small, represent parameter combinations that yield a reasonable match between experiment and simulation. These regions are somewhat broad and run diagonally across the parameter space, likely related to the qualitatively similar effects of γ and P on the time-independent size distributions. Specifically, the shape of the size distribution is determined by the relative rates of successful collisions between clusters at different sizes. When the magnitude of γ is large, larger clusters are less mobile and hence collide less frequently. However, collisions between larger clusters typically involve multiple contact points, and therefore have a high rate of success, when P is small, relative to collisions between smaller clusters. These competing factors cause size distributions obtained at large magnitudes of γ and small P to exhibit similar shapes as those obtained at small γ and large P. Note that this shape similarity only applies when comparing distributions at comparable mean cluster sizes and *not* comparable times, as the assembly dynamics are wildly different across the two sets of parameter combinations. As alluded to earlier, the shallowness in Q_ν may also result from the uncertainties in experimental $\nu_s(t)$ and from the CCA model being an oversimplification of the actual assembly process.

Despite the shallow concavity of the Q_ν-landscape, we are able to identify unique P-γ combinations that yield the closest overlap between simulation and experiment; these "predicted" values are marked by black boxes in Figure 3a. The simulated cluster size distributions corresponding to these parameter values and those obtained from experiments are provided in Fig. 3b. In particular, our approach predicts diffusivity scalings between $\gamma = -0.6$ and $\gamma = -0.8$ for all experiments except the one involving 30 nm spheres in 28k PS, where $\gamma = -0.9$ is predicted; even in this case, simulations with $\gamma = -0.8$ (and with the predicted P) yield a Q_ν value that is only marginally different (0.78 instead of 0.76) from that obtained with $\gamma = -0.9$. The predicted diffusivity scalings are mostly consistent with the Stokes-Einstein (SE) relationship, that is $D \sim 1/r$, where r is the cluster radius. Taking into account the fractal structure of the clusters, we have the relation $s \sim r^{d_f}$ between

cluster size and radius, where d_f is the fractal dimension. In our analysis of the experiment results, we found that $d_f \approx 1.4$ [12]; using this in the SE law yields $D \sim s^{-1/d_f} \approx s^{-0.7}$, consistent with our predicted γ. The SE relationship is generally applicable for particles that are much larger than the characteristic size of the surrounding polymer chains. Our calculations indicate that, indeed, our NPs, even the smallest ones (13 nm), are much larger than the radius of gyration R_g of the polymer chains ($R_g \simeq 3$ nm). To estimate R_g, we assumed that the PS matrix chains of Mw = 11k exhibit ideal chain conformations, and therefore $R_g \simeq b\sqrt{N/6}$, where $b \approx 20$ Å is the Kuhn length of PS and $N \approx 13.2$ is the number of such Kuhn segments in an 11k Mw PS chain [24]. That the diffusivity scaling exponent γ may be approximated as $-1/d_f$ was recently verified by molecular dynamics simulations of particle aggregates in a good solvent [25].

The predicted sticking probabilities P, on the other hand, vary dramatically across the experiments, ranging from $P = 0.001$ to $P = 0.4$. Remarkably, all five predicted values seem reasonable. Large 80 nm silver cubes should experience strong attractive inter-particle vdW forces, and we predict a sticking probability of $P = 0.4$ approaching unity for this species. Conversely, for the smallest particles studied (13 nm spheres) we obtain $P = 0.001$, the lowest value simulated. In the case of 10×40 nm rods and 30 nm spheres, sticking probabilities intermediate between these extremes are predicted, in keeping with the relative sizes of these particles. Among the two experiments with 30 nm spheres, the ones dispersed in longer matrix polymer exhibit a slightly higher sticking probability. This result is also reasonable, given that previous studies observe increased dewetting of individual polymer-grafted NPs as well as increased attraction between two such NPs with increasing length of the polymer matrix chains relative to the grafted chains [26]. It is also noted that the NP systems yielding relatively large P values (cubes, rods, and 30 nm spheres in 28k PS) yield cluster size distributions that develop a peak at large times, characteristic of diffusion-limited aggregation, whereas the remaining two systems with small P yield monotonically decreasing distributions at all times, consistent with reaction-limited aggregation [27].

While these extracted parameters paint a qualitative picture of the forces governing the assembly process and are also consistent with measured cluster size distributions, further work is required to quantitatively verify these results and to more rigorously validate our approach for extracting dynamic parameters. The former would require performing *in-situ* SEM studies of the above systems to observe the diffusion, collision, and sticking of NPs

in real time. The latter would require application of the approach to other self-assembling particulate systems for which the dynamic parameters are either known *a priori* or can be obtained from real-time visualization. Both these efforts are currently underway in our laboratories.

VI. VI. CONCLUSIONS

The results presented here demonstrate a simple and powerful approach for predicting dynamic parameters of NP assembly with several potential applications. First, the kinetic model, complete with its parameters, that emerges from the application of our approach should provide a comprehensive picture of the NP assembly process being studied. The predicted parameters could be used to explain experimental results in terms of dynamic processes and mechanisms. For instance, here we used the approach to provide evidence for the validity of the SE law in the polymer-NP systems examined and to determine whether they assembled via diffusion- or reaction-limited mechanisms. Second, the predicted parameters could inform researchers on how to modify aspects of the NP building blocks (e.g., length and density of polymer grafting that affect the stickiness P of the NPs) or the annealing conditions (e.g., time-modulation of temperature that affects D) to achieve specific higher-order structures. Third, the approach could be used to dissect the dynamical and mechanistic impact of the various experimental variables related to the NPs, the surrounding matrix, and the assembly conditions.

Our approach currently examines two-dimensional assembly of metal NPs within a polymer film and utilizes a CCA model to recover the dynamic parameters. However, the approach could be easily extended to other systems, including three-dimensional systems, and other kinetic models of assembly. Additional parameters accounting for effects like anisotropic interactions between NPs may also be incorporated within the CCA model. Also, we currently estimate the optimal dynamical parameters through brute-force comparison of experimental cluster properties with those obtained from a model simulated at hundreds of parameter combinations across the large parameter space. It should be possible to speed up the approach by automating the process of locating the global minimum in the Q_ν-landscape via optimization algorithms [28].

VII. ACKNOWLEDGMENTS

This work is supported by the National Science Foundation (CMMI, Grant No. 1200850), the American Chemical Society Petroleum Research Fund (Award No. 52515-ND7), and a Jacobs Graduate Fellowship to CRM.

---

[1] P. M. Ajayan, L. S. Schadler, and P. V. Braun, *Nanocomposite science and technology* (John Wiley & Sons, 2006).

[2] D. Maillard, S. K. Kumar, B. Fragneaud, J. W. Kysar, A. Rungta, B. C. Benicewicz, H. Deng, L. Cate Brinson, and J. F. Douglas, Nano Letters **12**, 3909 (2012).

[3] J. A. Fan, C. Wu, K. Bao, J. Bao, R. Bardhan, N. J. Halas, V. N. Manoharan, P. Nordlander, G. Shvets, and F. Capasso, Science **328**, 1135 (2010).

[4] B. Gao, G. Arya, and A. R. Tao, Nat. Nanotechnol. **7**, 433 (2012).

[5] B. R. Saunders, J. Colloid Interface Sci. **369**, 1 (2012).

[6] F. Family, P. Meakin, and T. Vicsek, J. Chem. Phys. **83**, 4144 (1985).

[7] D. A. Weitz, J. S. Huang, M. Y. Lin, and J. Sung, Phys. Rev. Lett. **54**, 1416 (1985).

[8] Y. Liu, X.-M. Lin, Y. Sun, and T. Rajh, J. Am. Chem. Soc. **135**, 3764 (2013).

[9] J. Park, H. Zheng, W. C. Lee, P. L. Geissler, E. Rabani, and A. P. Alivisatos, ACS Nano **6**, 2078 (2012).

[10] T. J. Woehl and T. Prozorov, J. Phys. Chem. C **119**, 21261 (2015).

[11] R. Podor, H.-P. Brau, and J. Ravaux, *In situ experiments in the scanning electron microscope chamber* (INTECH Open Access Publisher, 2012).

[12] C. R. Murthy, B. Gao, A. R. Tao, and G. Arya, Nanoscale **7**, 9793 (2015).

[13] P. Meakin, Phys. Rev. Lett. **51**, 1119 (1983).

[14] M. Kolb, R. Botet, and R. Jullien, Phys. Rev. Lett. **51**, 1123 (1983).

[15] P. Meakin, T. Vicsek, and F. Family, Phys. Rev. B **31**, 564 (1985).

[16] T. Vicsek and F. Family, **52**, 1669 (1984).

[17] M. L. Broide and R. J. Cohen, Phys. Rev. Lett. **64**, 2026 (1990).

[18] D. J. Robinson and J. C. Earnshaw, Phys. Rev. A **46**, 2045 (1992).

[19] P. H. F. Hansen and L. Bergström, J. Colloid Interface Sci. **218**, 77 (1999).

[20] C. R. Murthy and G. Arya, PICT: Particle image characterization tool, http://www.mathworks.com/matlabcentral/fileexchange/49382-pict--particle-image-characterization-tool.

[21] K. L. Gurunatha, S. Marvi, G. Arya, and A. R. Tao, Nano Lett. **15**, 7377 (2015).

[22] M. Kolb and R. Jullien, J. Physique Lett. **45**, L-977 (1984).

[23] The probability $P_{\text{no-stick}}$ that two clusters do *not* stick is given by the probability $1 - P$ that each of the c contacts do not stick, yielding $P_{\text{no-stick}} = (1 - P)^c$. Given that the probability P_{stick} that the two clusters stick is given by $1 - P_{\text{no-stick}}$ implies that $P_{\text{stick}} = 1 - (1 - P)^c$.

[24] J. S. Pedersen and P. Schurtenberger, Europhys. Lett, **45**, 666 (1999).

[25] G. Pranami, M. H. Lamm, and R. D. Vigil, Phys. Rev. E **82**, 051402 (2010).

[26] D. M. Trombly and V. Ganesan, J. Chem. Phys. **133**, 154904 (2010).

[27] D. A. Weitz and M. Y. Lin, Phys. Rev. Lett, **57**, 2037 (1986).

[28] D. Meluzzi and G. Arya, Nucleic Acids Res. **41**, 63 (2013).